Quantum control of electron wave packets in bound molecules by trains of half-cycle pulses

Emil Persson,[1] Markus Pichler,[1] Georg Wachter,[1] Thomas Hisch,[1] Werner Jakubetz,[2]
Joachim Burgdörfer,[1] and Stefanie Gräfe[1,*]

[1]*Institute for Theoretical Physics, Vienna University of Technology, Wiedner Hauptstr. 8-10, A-1040 Vienna, Austria*
[2]*Institute for Theoretical Chemistry, University of Vienna, Währingerstr. 38, A-1090 Vienna, Austria*

(Received 12 August 2011; revised manuscript received 5 September 2011; published 19 October 2011)

We investigate protocols for transient localization of electrons in homodiatomic molecules, as well as permanent localization via population inversion in polar molecules. By examining three different model systems with one electronic and one nuclear degree of freedom, we identify mechanisms leading to control over the localization of the electronic wave packets. We show that electronic states dressed by the quasi-dc component of the train of half-cycle pulses steer the combined electronic and nuclear motion toward the targeted state.

DOI: 10.1103/PhysRevA.84.043421 PACS number(s): 32.80.Qk, 33.80.−b, 82.50.Nd, 82.50.Pt

I. INTRODUCTION

In the last two decades, many different quantum control protocols have been developed and implemented with the goal to steer the quantum system toward a selected target state [1,2]. Most of the applications focus on controlling the nuclear dynamics, accessible on the femtosecond time scale [3–7]. Extending these concepts from the regime of femtosecond molecular chemistry to the realm of electronic dynamics on the attosecond scale has remained a challenge and is still in its infancy. Since the controlling pulse is in many cases of attosecond duration, its spectrum extends into the XUV domain leading, almost inevitably, to ionization.

Quantum control schemes to steer the dynamics of ionized ("free") electrons have been suggested, using either intense two-color laser fields [8,9] or, alternatively, the ellipticity [10,11] of a single-color laser field. For bound electrons, different approaches to obtain control over the electronic dynamics have been proposed. In atoms, selective population of field-dressed states has been implemented experimentally [12] as well as stimulated Raman adiabatic passage and its relatives [13]. In molecular systems, the exertion of control of electronic dynamics can be mainly divided into two classes: to (i) "shape" (field-dressed) electronic states (bound or dissociative) to indirectly control the nuclear dynamics [14,15], or to (ii) steer the localization dynamics of an electron upon dissociation [16–26]). The latter works mainly employed the control over the carrier-envelope phase of the intense few-cycle laser pulses, or over the timing of the controlling laser pulse [18,20,21]. In another approach by Gräfe and Engel [27], a quantum control algorithm is applied to the coupled nuclear-electronic dynamics of a model system with bound electronic states by phase and amplitude shaping the electric field directly.

Linearly polarized, single-color laser pulses containing a large number of cycles are inversion symmetric relative to the laser polarization axis. This inversion symmetry poses limitations on control schemes since target states with broken inversion symmetry are out of reach. Carrier-envelope phase stabilized, few-cycle infrared pulses break the inversion symmetry resulting in a large asymmetry in the yield of electrons from atoms [28–30] and in the dissociation fragments from small molecules [16]. Alternatively, if both odd and even harmonics of the fundamental driving field are present, inversion symmetry of the field can be broken. Combining several harmonics with phase-locked colors, a train of unidirectional half-cycle pulses (HCPs) can be generated. Half-cycle pulses and trains of half-cycle pulses have proven to be useful tools in quantum control. They steer dissociation dynamics [31,32], isomerization reactions [17,33], and orient rotational wave packets [34,35]. On longer time scales, trains of HCPs have been applied to control the dynamics of Rydberg wave packets in atoms [36–39]. Very recently, we have shown that trains of HCPs can control the coupled nuclear-electronic dissociation dynamics of H_2^+ [25] and a high degree of asymmetry of dissociation can be reached.

In this work, we address the more challenging goal of controlling electron localization in bound rather than dissociating molecular systems by trains of HCPs. The conceptual difficulty with steering electronic wave packets in systems that remain bound originates from the fact that the electronic motion cannot be easily arrested (or "frozen out") as it happens in a dissociating molecule. Localization of the electronic wave packet is therefore either transient in symmetric potentials or can be made permanent if the electron is steered toward a strongly polarized stationary state in asymmetric potentials.

The ultimate goal of bound-state electron steering is a light-wave controlled electron current, e.g., along a chain molecule, or the transient spatial localization to induce detachment of a targeted functional group. As a first step in this direction, we explore steering of electronic wave packets in diatomic molecules. We consider three different model potentials representing diatomic molecules where the two lowest electronic states are bound: (I) a homonuclear case with a very small gap between two bound electronic states, (II) a homonuclear case with a large gap, and (III) a model for an asymmetric potential, where either the nuclear charges or masses differ. We explore the mechanism underlying electron localization in bound systems and show the limitations. In molecules with a small energy gap between the two electronic states, efficient transient localization can be obtained. For molecular model systems with a larger energy gap, only limited localization can be found; however, population inversion could be obtained in these systems. In asymmetric potentials, population inversion is analogous to electron localization and can be obtained very

*stefanie.graefe@tuwien.ac.at

efficiently. While detection of localization in heterodiatomic molecules can be accomplished by spectroscopic methods, probing transient localization requires ultrafast pump-probe techniques, e.g., by applying an attosecond XUV pulse at variable delay times during the interaction with the driving HCP train, and measuring the forward-backward asymmetry in the energy-resolved photoelectron distribution [40].

The paper is organized as follows: Sec. II briefly describes the model systems representing molecules with nondissociative excited electronic states. In Sec. III the numerical results for quantum control of electronic localization dynamics in bound systems are presented, together with a description of the underlying physical mechanism. Finally, Sec. IV contains a brief summary and conclusions.

II. BRIEF DESCRIPTION OF THE THEORETICAL METHODS

A. Model for bound molecular systems

As a model system, we consider the coupled nuclear-electronic dynamics of prototype model systems representing simple diatomic molecular ions. These model systems are parameterized such that the two lowest lying electronic states of the model system are bound states with even and odd symmetry. We consider both homonuclear and heteronuclear molecules (Fig. 1). The model potentials are constructed by one-dimensional soft-core potentials with a smoothing function $\alpha(R)$ depending on the nuclear degree of freedom R applied. The Hamiltonian of this system with one electronic degree of freedom ($-\infty < x < \infty$) and one nuclear degree of freedom ($0 \leqslant R < \infty$) is given by the sum of kinetic $\hat{T}$ and potential V terms and the interaction with the external field $E(t)$:

$$\hat{H} = \hat{T}_x + \hat{T}_R + V(x,R) + xE(t), \tag{1}$$

$$V(x,R) = +\frac{1}{R} + V_+(x,R) + V_-(x,R),$$
$$V_\pm(x,R) = -\frac{1}{\sqrt{(x \pm R/2)^2 + \alpha^\pm(R)}}. \tag{2}$$

Variation of the smoothing function $\alpha^\pm(R)$ allows us to control the equilibrium internuclear distance, the energy gap between the electronic states, and the ionization potential.

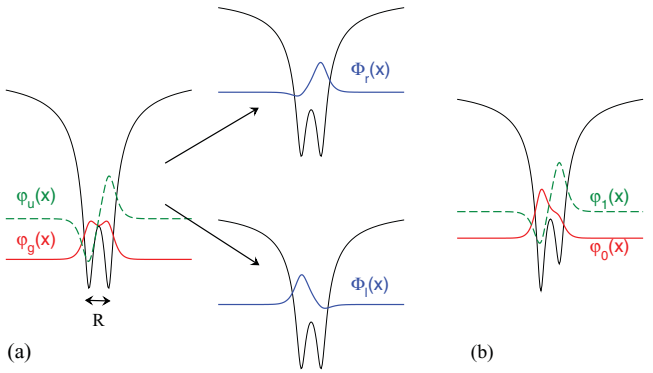

FIG. 1. (Color online) Electronic model potentials $V(x,\bar{R})$ and eigenfunctions at fixed internuclear distances $\bar{R} = 2$ Å for (a) symmetric and (b) asymmetric potentials.

For homonuclear molecules, $\alpha^+ = \alpha^- = \alpha$ (Fig. 1), while the two functions differ for the asymmetric case where the nuclei have different charges. We have also examined the possibility to control electron localization in heteronuclear systems, where the masses but not the charges of the two nuclei differ ($m_1 \neq m_2; m_1 + m_2 = m_{\rm tot}$). Such molecules are represented in the center of mass frame by the following potential

$$V(x,R) = +\frac{1}{R} - \frac{1}{\sqrt{\left(x - \frac{m_1}{m_{\rm tot}}R\right)^2 + \alpha(R)}} - \frac{1}{\sqrt{\left(x + \frac{m_2}{m_{\rm tot}}R\right)^2 + \alpha(R)}}. \tag{3}$$

The dipole interaction term in Eq. (1) becomes

$$+\left(x - \frac{m_2 - m_1}{m_{\rm tot}}R\right)E(t). \tag{4}$$

The particular choice of smoothing function $\alpha(R)$ will be given below. Certainly, within this reduced dimensionality model some physical problems such as the dependence on the relative orientation between the internuclear axis and the external field axis cannot be addressed. However, for linearly polarized fields and dynamics developing mainly along the molecular axis, the relevant features can be extracted from a one-dimensional description. A full three-dimensional calculation might yield different absolute values for the absolute asymmetry but would most likely not fundamentally alter the underlying mechanisms.

We solve the time-dependent Schrödinger equation (TDSE) for the coupled electronic and nuclear coordinate

$$i\frac{\partial}{\partial t}\Psi(x,R,t) = \hat{H}\Psi(x,R,t), \tag{5}$$

subject to the initial conditions

$$\Psi(x,R,t=0) = \varphi_g(x;R)\,\chi_0(R). \tag{6}$$

In Eq. (6), $\varphi_g(x;R)$ is the gerade electronic eigenstate (ground state), and $\chi_0(R)$ the vibrational ground state. The calculations are performed on a two-dimensional grid, using the split-operator technique [41] with typical grid parameters as follows: a total number of 512 points in R and 1024 in x, where the grid in R is defined from 0.1 to 32 a.u., and the grid in x from -100 to 100 a.u.

While the exact grid-based numerical solution does not involve Born-Oppenheimer (BO) states, it is, nevertheless, instructive to perform calculations within the basis expansion of the two lowest Born-Oppenheimer states, the gerade and ungerade states, resulting in the nuclear Schrödinger equation

$$i\frac{\partial}{\partial t}\begin{pmatrix}\chi_g(R,t)\\ \chi_u(R,t)\end{pmatrix} = \hat{H}_{\rm nucl}\begin{pmatrix}\chi_g(R,t)\\ \chi_u(R,t)\end{pmatrix}, \tag{7}$$

with the nuclear Hamiltonian

$$\hat{H}_{\rm nucl} = \left[-\frac{1}{2M}\frac{\partial^2}{\partial R^2}\mathcal{I} + \begin{pmatrix}V_g(R) & -\mu_{gu}(R)E(t)\\ -\mu_{gu}(R)E(t) & V_u(R)\end{pmatrix}\right]. \tag{8}$$

Here, M is the reduced nuclear mass, $\mathcal{I}$ is the unit matrix, and $\mu_{gu}(R)$ is the transition dipole between the ground and the upper electronic states. The potential curves $V_g(R)$ and $V_u(R)$ are the electronic eigenenergies, parametrically depending on R. The calculations within the Born-Oppenheimer basis expansion are implemented primarily for time-consuming scans in the multidimensional control parameter space. The control fields obtained serve then as an input for the subsequent analysis within the full numerical solution of the TDSE.

Moreover, for analysis the wave functions resulting from the full calculations are expanded into the basis of Born-Oppenheimer states,

$$\Psi(x,R) = \sum_i c_i\, \varphi_i(x;R)\, \chi_i(R), \tag{9}$$

where the $\varphi_i(x;R)$ are the electronic eigenstates, and the $\chi_i(R)$ are the nuclear wave functions. Observables to be extracted include the time-dependent populations $P_{g,u}(t) = |\langle \varphi_{g,u}|\Psi(t)\rangle|^2$ of the gerade and ungerade states, the bond length expectation values $\langle R(t)\rangle = \langle \Psi(t)|R|\Psi(t)\rangle$, and—in the context of localization dynamics in homonuclear systems—the projections onto the "left" (l) and "right" (r) coherent superposition states, $P_{r,l}(t) = |\langle \Phi_{r,l}|\Psi(t)\rangle|^2$, with

$$\Phi_r(x,R) = \frac{1}{\sqrt{2}}[\varphi_g(x,R) + \varphi_u(x,R)], \tag{10}$$

$$\Phi_l(x,R) = \frac{1}{\sqrt{2}}[\varphi_g(x,R) - \varphi_u(x,R)]. \tag{11}$$

For large R, these superposition states converge to the localized atomic wave functions in the right or left potential well, i.e., the two dissociation limits $X^+ + X$ and $X + X^+$. We quantify the degree of localization by the (time-dependent) asymmetry coefficient

$$A(t) = \frac{P_l(t) - P_r(t)}{P_l(t) + P_r(t)}. \tag{12}$$

The domain of the asymmetry function extends from -1 to $+1$, where the sign indicates the direction in which the electron is preferentially localized. Localization in the direction of the force exerted by the unipolar peak field of the HCP train (positive fields) yields localization in the left potential well, i.e., $A > 0$. As we consider bound states and the molecule is not dissociating, localization—as defined by Eq. (11)—can be permanent for heterodiatomic and polar molecules but only transient for homonuclear molecules. We will maximize A via the application of a genetic algorithm to optimize the control parameters of the pulse train.

B. Half-cycle pulses

Trains of HCPs consist of a sequence of ultrashort unipolar electric field "spikes." Propagating electromagnetic fields must satisfy the requirement $\int E(t)dt = 0$. Therefore, the peak field in one direction ("kicks"), $E_+(t)$, is accompanied by a low-amplitude quasi-dc offset field in the opposite direction, $E_-(t)$.

Such pulses can be generated by techniques based on harmonic generation [42,43], promising HCP trains down to the attosecond regime [25]. The HCP train can be synthesized by the superposition of harmonic colors

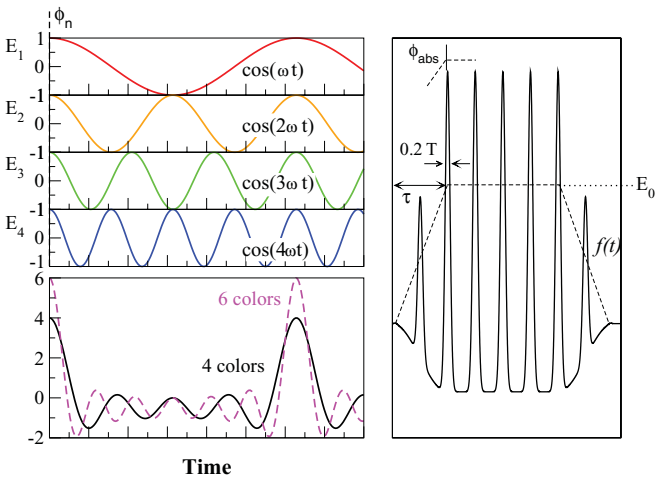

FIG. 2. (Color online) Formation of unidirectional half-cycle pulse trains by superposing harmonic colors $n\omega$ to the fundamental frequency ω with appropriate phase ϕ_n and amplitude $E_n = E_0\theta(6-n)$ (left panel). In general, $|E_n| \to 0$ as $n \to \infty$. In addition, the envelope function $f(t)$ can be optimized. An example of a HCP used in localization protocols is shown in the right panel.

$$E(t) = E_0\, f(t)\left(\sum_n E_n \cos(n\omega t + \phi_n)\right), \tag{13}$$

where $f(t)$ is the normalized envelope function, E_0 the overall field strength, and E_n the amplitude of the harmonics with phase ϕ_n. Mixing the fundamental frequency ω_1 with several higher (even and odd) harmonics and choosing the phases ϕ_n properly, a unidirectional HCP train can be formed (Fig. 2). In our simulations, we mixed six harmonic colors (thereby defining the width of the kicks to be 0.2 periods) and chose a flat-top envelope function with a smoothed ramp-on and -off. Accordingly, the offset field $E_-(t)$ is given by

$$E_-(t) = -E_0\, f(t)/2\,. \tag{14}$$

Trains of HCP's have, indeed, been generated experimentally very recently; see, e.g., [44,45]. Novel light sources in the far infrared with higher power promise to pave the way toward subfemtosecond half-cycle pulse trains as used in the following.

III. NUMERICAL RESULTS

The objective is to find optimally shaped pulse trains which in the diatomic molecules induce the highest possible degree of electron localization in one potential well. We consider both inversion-symmetric electronic potentials [Fig. 1(a)] representing homonuclear molecules and asymmetric potentials [Fig. 1(b)]. The asymmetric potentials we consider consist of two nuclei with the same mass but different charges. We have also analyzed heteronuclear molecules where the nuclear masses differ. The unidirectional HCP train with a predefined direction of force should induce localization of the electronic wave packet near one of the two potential wells. Unlike for dissociative systems, where degenerate

dissociative states of opposite inversion symmetry exist and, thus, asymmetric and localized final states can be formed [25], the quest for localization of wave packets in bound molecules is fundamentally different. For asymmetric potentials [Fig. 1(b)], localization entails stepwise the wave packet toward a targeted (in general, excited) electronic eigenstate with the desired localization properties. For inversion-symmetric potentials [Fig. 1(a)], on the other hand, localization will be transient and persists only as long as the symmetry-breaking HCP is present. The physical significance of transient localization lies in the fact that it can trigger the formation or breaking of bonds, e.g., of functional groups attached to chain molecules.

The pulse train we are searching for will in most cases induce localization in the direction of the force of the HCPs. However, localization in the opposite direction along the direction of the quasistatic dc field is possible as well, as will be shown below. The parameters of the HCP train optimized by the genetic algorithm are the fundamental frequency ω, the field strength E_0, the absolute phase of the generating fundamental pulse $\phi_{\rm abs}$, and the rise time τ, corresponding to the time needed to reach the maximum value of the flat-top envelope [Fig. 2(b)]. The length of the pulses is kept constant, and the width of the kicks was fixed to $0.2T$.

All results presented are obtained from the fully coupled nuclear-electronic system. Only the search for optimal values of the control parameters with the genetic algorithm are performed within the framework of the BO expansion for reasons of computational efficiency.

A. Inversion-symmetric potential

We consider first the case of an inversion-symmetric potential. All electronic eigenstates have well-defined inversion symmetry. Symmetry breaking localization is therefore only possible in the presence of an HCP. The efficiency in forming a transiently localized wave packet obviously depends on the energy gap between two nearby eigenstates of opposite inversion symmetry. We therefore consider first a model potential, referred to as potential (I), for which the excitation gap to the first excited state is very small and the equilibrium internuclear distances in those two states are very similar (in this simulation we set the mass equal to the proton mass). The smoothing function $\alpha(R)$ entering the nuclear-electron potential [Eq. (1)] is parameterized as follows:

$$\alpha(R) = \begin{cases} a e^{-(R-r_1)^2/a_1^2}, & R < R_c \\ b + \frac{c}{1+e^{-(R-r_2)/a_2}}, & R \geqslant R_c \ . \end{cases} \qquad (15)$$

The potentials in Fig. 3 result from the following choice of parameters: $a = 0.6055$, $r_1 = 5$, $a_1 = 4.24$, $b = 0.6$, $c = 0.825$, $r_2 = 6.75$, $R_c = 5$, and $a_2 = 0.35$. A measure for the size of the excitation gap is the ratio of zero-field spacing $|V_u(R_{\rm eq}) - V_g(R_{\rm eq})|$ at the equilibrium distance $R_{\rm eq}$ to the energy shift induced by the dressing by the weak quasi-dc component of the HCP. In the present case, this ratio is of the order of unity.

The optimal pulse train maximizing the asymmetry $A(t)$ found after less than 50 generations has a field strength of $E_0 = 0.012$ a.u., a rise time τ of two optical cycles, a wavelength of 949 nm, and phase $\phi_{\rm abs} = 0$ (i.e., one HCP spike lies directly at the position where the ramp-on of the envelope has reached its maximum); see Fig. 4, upper panel. The electronic density distribution [Fig. 4, lower panel] develops already during the ramp-on a pronounced asymmetry with charge displacement in the direction of the force exerted by the HCP "kicks." Thus, localization persists while the HCP train continues. Counterintuitively, during the periodic kicks a small fraction of the electronic density can be found on the opposite site of the molecule. After the end of the pulse train, localization of the charge density is replaced by oscillations. Concurrently, with the excitation of the electronic wave packet, also a vibrational (nuclear) wave packet, starting from the ground state, is initiated (Fig. 5). The fact that the bond-length expectation value exhibits oscillations with a

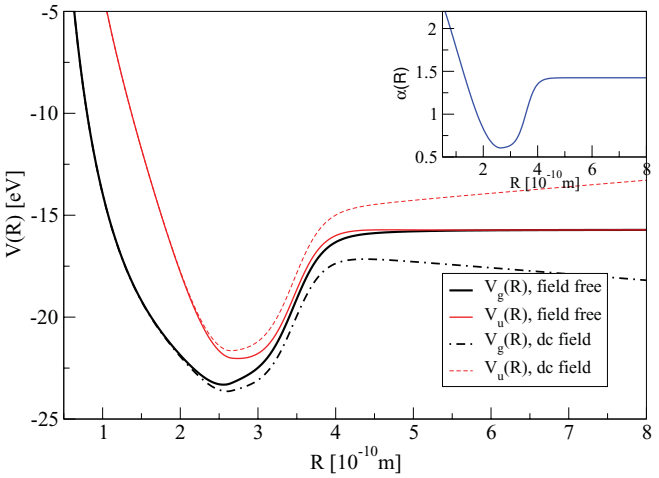

FIG. 3. (Color online) Two lowest lying Born-Oppenheimer potential curves for potential (I) with a small excitation gap with and without a dc field of strength 0.012 a.u. present. Inset: smoothing function $\alpha(R)$.

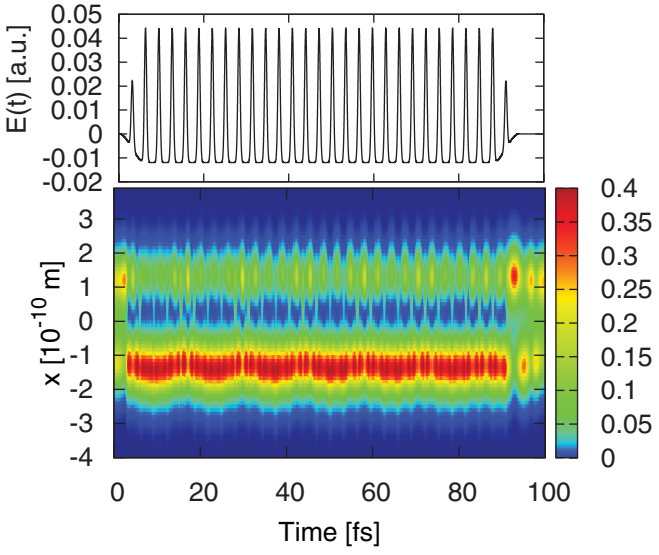

FIG. 4. (Color online) Model potential (I): electronic density $\varrho(x,t) = \int |\Psi(x,R,t)|^2 dR$ of system (I) in the presence of the HCP field (lower panel). The upper panel displays the HCP field found by the genetic algorithm when optimizing for localization.

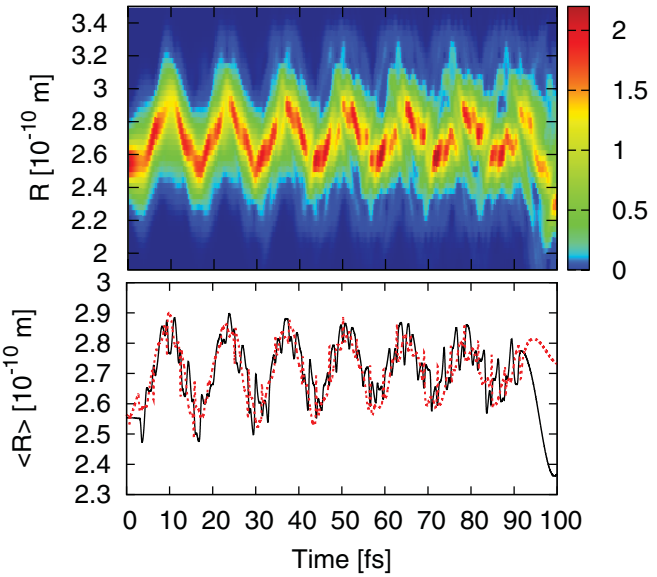

FIG. 5. (Color online) Nuclear density $\varrho(R,t) = \int |\Psi(x,R,t)|^2 dx$ of system (I) (upper panel), and bond-length expectation values $\langle R(t)\rangle$ in the gerade (black line) and ungerade electronic states [red (dotted) line] (lower panel) in the presence of the HCP field.

well-defined frequency is an obvious consequence of the very similar shape of the two adiabatic potential curves giving rise to oscillations in $\langle R_g(t)\rangle$ and $\langle R_u(t)\rangle$ closely mirroring each other. While significant population transfer occurs between the lowest two electronic states, excitation to high-lying states or ionization is negligible ($< 0.6\%$). Consequently, the two-state Born-Oppenheimer basis expansion [Eq. (7)] is well justified in this case. A high degree of localization can be achieved: more than 80% of the population can be driven into the state $\Phi_l(x,R)$, corresponding to A ≈ 0.6 [Fig. 6(b)]. Moreover, on top of the localization dynamics, a modulation with a time scale

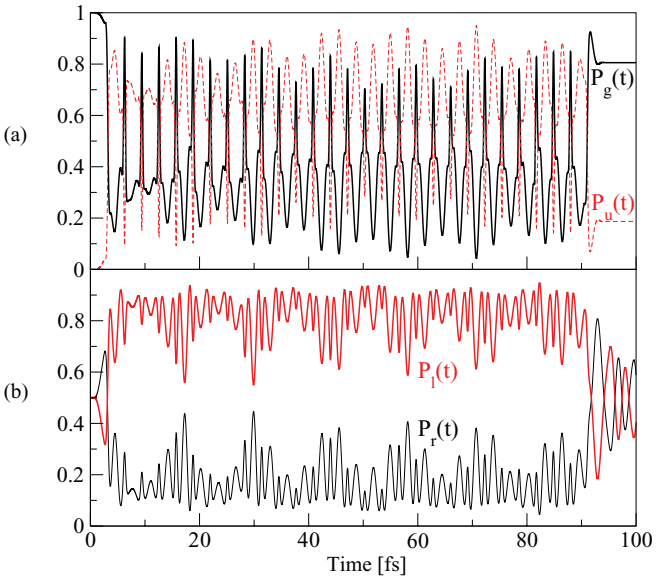

FIG. 6. (Color online) (a) Population transfer $P_g(t), P_u(t)$ and (b) localization $P_l(t), P_r(t)$ for model molecule (I).

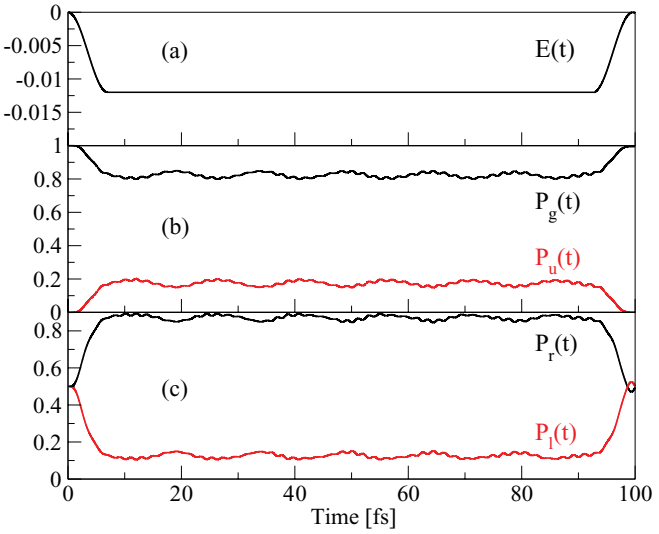

FIG. 7. (Color online) (a) Evolution of system (I) driven by a slowly varying quasi-dc field of strength 0.012 a.u.: (b) population transfer dynamics and (c) localization dynamics.

of 18 fs can be observed, signifying the vibrational dynamics of the nuclear wave packet.

The origin of the efficient localization lies in the interplay between the kicks and the quasi-dc field pointing in opposing directions. To highlight the latter, we first repeated the simulation switching off the negative offset component of the field. While population transfer and nuclear wave packet dynamics persist, the electron localization disappears. We have then taken the opposite limit and followed the dynamics within the framework of field-dressed states, taking into account the quasi-dc offset field only. Since this field is only slowly varying in time, we can consider the system as adiabatically moving in the field-dressed states of the offset field, while the kicks almost impulsively drive transitions between the field-dressed states. A similar picture was found useful to explain the electron localization in the dissociative dynamics of H_2^+ [25]. The field-dressed states are the eigenstates of the Hamiltonian

$$H_{\rm dc} = \hat{T}_x + \hat{T}_R + V(x,R) + xE_-(t). \qquad (16)$$

The resulting adiabatic electronic eigenenergies are also displayed in Fig. 3. Repeating the time-dependent simulation with the slowly varying offset component, keeping other parameters fixed, results in very efficient localization with up to 90% of the electronic density now in the *right* rather than the *left* potential well, see Fig. 7. Increasing the field strength and increasing the length of the ramp-on and -off, close to 100% in the superposition state Φ_r can be reached (figure not shown). The electron is driven adiabatically by the offset field into the right potential well, which is not an eigenstate of the field-free system. Therefore, as soon as the field is switched off, the electron density will revert to φ_g. The time scale of the envelope function $f(t)$ which governs the offset field [Eq. (14)] would correspond to a half cycle of a terahertz pulse. Such a field can be considered as unidirectional on the natural time scale of a small molecule, thereby inducing transient localization of the electron. Clearly, by a multicycle

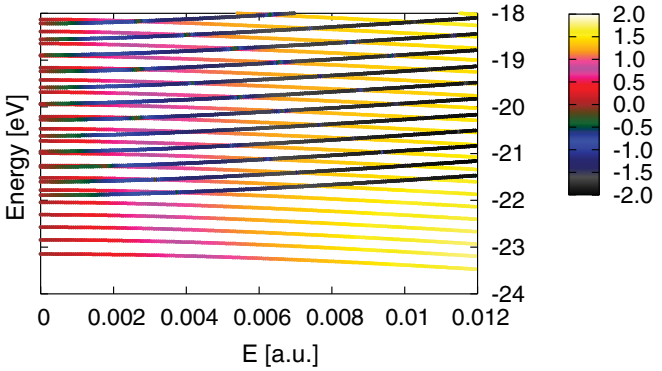

FIG. 8. (Color online) Energy of field-dressed vibronic states with quantum number ν_{dc} as a function of field strength. The color indicates the degree and direction of polarization.

terahertz pulse the charge density could be periodically driven between different centers of localization.

In order to analyze the mechanism for transient localization by the HCP train, i.e., in the presence of both the slowly varying offset field and the kicks, we follow the dynamics in terms of the offset field-dressed vibronic Born-Oppenheimer states evaluated at the instantaneous field strength (Fig. 8). States oriented in the direction of the kicks are energetically disfavored while those states oriented in the direction of the offset component are energetically lowered. The population dynamics (Fig. 9) illustrates the interplay between adiabatic following and sudden kick-induced transitions. After initial polarization in the direction of the quasi-dc field during the ramp-on pulse, a kick at $t = 3$ fs transfers close to 100% of the population to very few high-lying states around vibrational quantum number $\nu_{dc} = 9$, polarized in the direction of the kicks. At $t = 6$ fs the driving field has reached its full strength. Subsequently, the kick has twice the amplitude compared to the kick at $t = 3$ fs. This and all following kicks are no longer efficient in transferring significant amounts of the population into other states. The system remains predominantly in the single field-dressed vibronic state $\nu_{dc} = 9$. This state is not only the one which is lowest lying field-dressed state for a field polarized in the direction of the kicks, but also the one matching the dynamical time scale in the upper potential well. As only a few vibrational states are populated, the nuclear wave packet dephases only slowly and remains well localized over several vibrational periods.

The physical process uncovered by the genetic algorithm can be summarized as follows. One kick is placed at the optimal time for an almost perfect sudden transfer from the lower to the upper offset-field dressed states. The transfer occurs for internuclear distances R confined to a relatively narrow interval $2.5\text{Å} \leqslant R \leqslant 3\text{Å}$. Within this interval, the characteristic parameters of the dressed electronic potential curves involved, the energy spacing, and their gradient remain unchanged. Moreover, as the vibrational wave packets in both states are moving synchronously, transient localization can be very efficient for long times, covering many vibrational periods.

The same localization dynamics with nearly the same efficiency is observed when varying the reduced nuclear mass. We expect this mechanism to be operative for diatomic molecular systems, where the two lowest lying electronic states with opposite symmetry have closely aligned equilibrium internuclear distances such that field dressing can simultaneously adjust the shape of both potentials, thereby synchronizing the nuclear dynamics. The ratio of zero-field spacing $|V_u(R_{eq}) - V_g(R_{eq})|$ at the equilibrium distance R_{eq} to the energy shift induced by the dressing by the weak quasi-dc component of the HCP is of the order of unity.

The strong dependence of the transient localization dynamics on the properties of the electronic potential curves is highlighted by a simulation for a homodiatomic system with a larger energy spacing between the two lowest-lying states of opposite inversion symmetry, referred to in the following as model system (II). We chose potential curves and masses to resemble the oxygen molecular ion, O_2^+. We use the functional form Eq. (15) for the smoothing functions with parameters $a = 1.017$, $r_1 = 3.95$, $r_C = 3.95$, $a_1 = 4.24$, $b = 1.0$, $c = 0.925$, $r_2 = 6.35$, and $a_2 = 0.6$. The resulting Born-Oppenheimer potential curves (Fig. 10) feature not only a larger energy spacing but also significant displacement of the equilibrium internuclear distance for the two electronic states. This immediately suggests that the nuclear dynamics is not easily synchronized in those potential wells in the presence of the realistic (moderate) field strength of the HCP train. Indeed, running the genetic algorithm within the two-state Born-Oppenheimer approximation yields similar strong

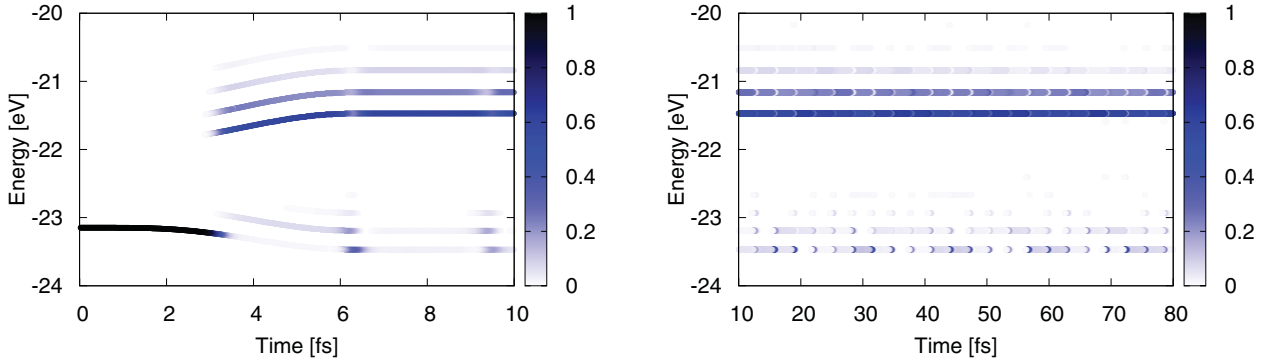

FIG. 9. (Color online) Population dynamics in the basis of offset field-dressed vibronic states: in the early stage (left panel), the kick near $t = 3$ fs transfers population into the field-dressed state $\nu_{dc} = 9$, where it remains during the further interaction with the HCP train almost unperturbed by the kicks. The right panel shows the long term behavior of the system during the interaction of the pulse train.

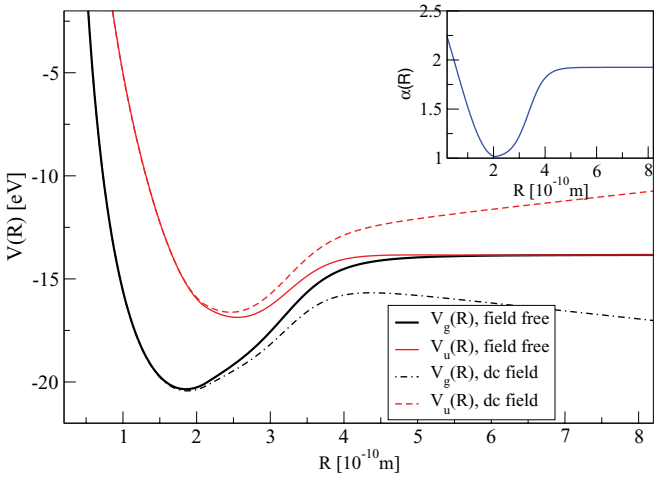

FIG. 10. (Color online) Two lowest-lying Born-Oppenheimer potential curves of model system (II) with large excitation gap with and without a dc field of strength 0.015 a.u. present. Inset: smoothing function $\alpha(R)$.

electron localization only at significantly higher field strengths. However, in the full nuclear-electronic calculation, substantial ionization as well as significant population transfer to higher-lying electronic states occurs, excluding such pulses from further consideration. Restricting the range of the permitted field strengths within the genetic algorithm leads to less successful optimization, an example of which is shown in Fig. 11.

Moderate levels of localization are accomplished, however, at the price of significant ionization (≈30%). One key difference to case (I) with a small excitation gap is the reduced efficiency in reaching population inversion. While in the previous case, population inversion is achieved by the first two kicks, due to the much larger gap between the

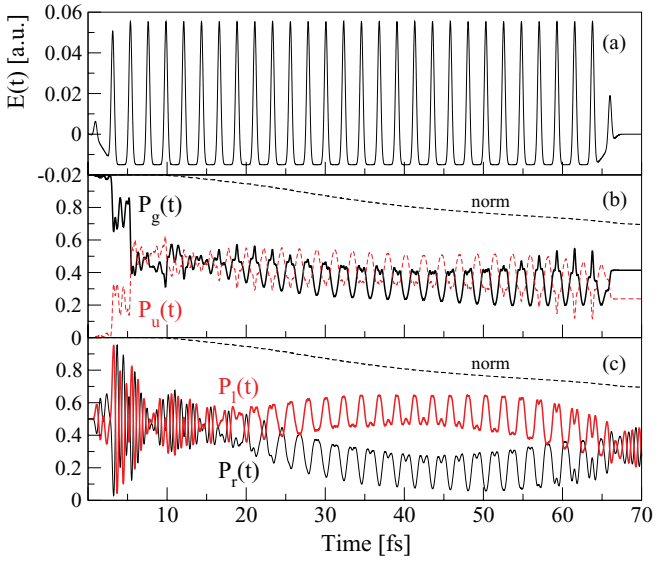

FIG. 11. (Color online) (a) Evolution of system (II) driven by the HCP field: (b) population transfer dynamics and (c) localization dynamics. The dashed line displays the norm $\int |\Psi(t)|^2 dx\, dR$ of the wave function.

electronic states, population transfer requires either higher field strengths or a stepwise population transfer. The problem with such a stepwise excitation is that with each step, a new nuclear wave packet in the upper state is created and thereby the phases between the electronic wave functions in the two electronic states $[\phi_g(x,R) \pm \phi_u(x,R)]$ cannot be locked. Thus, population transfer can be achieved, but localization cannot. The algorithm is forced to higher field strengths, where population transfer to the upper state occurs on short time scales (driven by the third harmonic color of the driving field, which is almost resonant with the energy gap) and similar nuclear dynamics in both electronic states can proceed. At $t = 40$ fs, both wave packets are located at similar internuclear distances around the outer turning point ($R = 3$Å), where the electronic gap is smaller, and localization is obtained.

An alternative strategy would be to employ the slowly-varying offset field corresponding to half-cycle terahertz pulse. In this case, ionization is strongly suppressed even though the fields strength of the quasi-dc component is increased by a factor of 2 compared to that of the HCP train. The highest degree of localization is observed at larger times, when the nuclei have reached the outer turning point. Again, after the pulse is over, virtually no population is transfered to the ungerade electronic state.

To summarize the findings for model system (II): because of the large excitation gap, transient localization by a HCP train requires field strengths that lead to strong ionization. As a viable alternative, near-adiabatic polarization in the presence of a terahertz half-cycle pulse emerges which, however, leaves the system in its ground state after the interaction with the pulse.

B. Model System (III)—Broken inversion symmetry

In asymmetric potentials the inversion symmetry is broken in the absence of the field. Consequently, electronic and vibrational states are inherently polarized. We consider two types of asymmetric potentials; the first class are homonuclear diatomics, where one nucleus has a different charge than the other, and the second class are heterodiatomics with two different masses. The ground state in asymmetric potentials is polarized in the direction of the deeper well while the upper one is polarized in the opposite direction of the shallower well (Fig. 12). Hence, excitation to the upper state is equivalent to reversing the localization of the electron. Therefore, the genetic algorithm searches for an efficient strategy to transfer population to the upper state [maximize $P_l(t \to \infty)$], reversing the direction of polarization.

We simulate polar diatomic molecules by setting $\alpha^+(R) = \alpha^-(R) - 0.3$ (Fig. 12). The atomic mass is kept at 16 amu., and $\alpha(R)$ is chosen to be the same as for model system (II). This represents systems where one of the nuclei has a higher effective charge than the other. Intuitively, one expects that population transfer into a predefined potential well is now mitigated by a polarized driving field. As the initial vibronic states are already polarized, the direction of the driving field pushes the wave packet either in the "right" or the "wrong" direction. Consequently, reversing the polarity of the previously optimized HCP will not induce any significant population transfer. The resulting electron dynamics (Fig. 13)

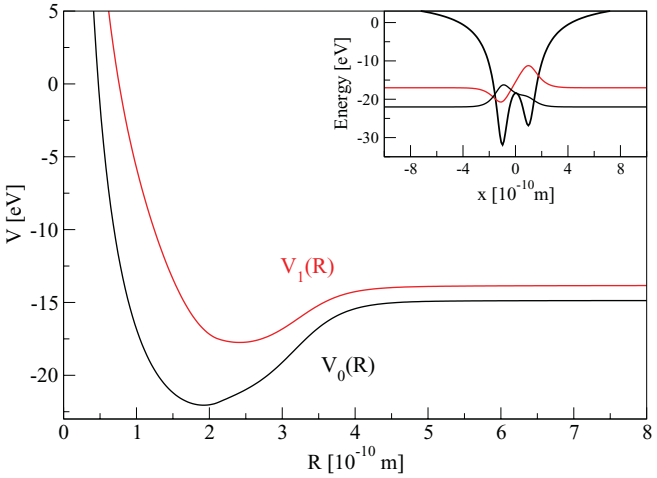

FIG. 12. (Color online) Born-Oppenheimer potential curves of the polar model system (III) with broken inversion symmetry. The inset shows a cut of the full electronic potential for a fixed value of the internuclear distance $R = 2$Å with the two lowest electronic eigenfunctions.

in the HCP field found by the genetic algorithm displays population inversion and, hence, localization on the other nucleus. The population transfer proceeds in a stepwise manner [46,47]. Overall, the population inversion is very efficient; over 90% of the population is transferred to the upper electronic state without substantial losses to other electronic states or ionization. The field strength of the optimal field is very low, as dipole coupling to the field is very strong and the states are easily polarizable.

It is also of interest to compare the control achieved with the train of HCPs with that of the offset field only. Using the same strength of the offset field as present for the HCP train (i.e., $E_- = -0.0125$ a.u.; see Fig. 13) leads to less than 1% population transfer into the upper state. Increasing the field strength, more population can be transferred. For the offset field, both the reversal of localization and the population transfer to the upper state are transient. The population reverts to the ground state as E_- is adiabatically switched off. We note that the control of the population transfer by the HCP (Fig. 13) can be extended to a selective population of vibronic states on the electronically excited state. This can be realized by adding an additional constraint to the genetic algorithm to selectively populate the vibrational ground state or one of the low-lying excited vibrational state in the upper electronic state. In contrast, steering toward high-lying vibronic states is less successful.

We note that this population inversion in asymmetric potentials is also very efficient when only two colors form a HCP-like train, substantially simplifying possible experimental realizations.

The second class of systems with broken inversion symmetry are heterodiatomic molecules, where one nucleus has a larger mass than the other, thereby featuring a permanent dipole moment. Heteronuclear molecules are given by the potential in Eq. (3). First, we have repeated the calculation for model system (I) with the small gap but doubled the mass of one of the nuclei. Applying the same control field as in

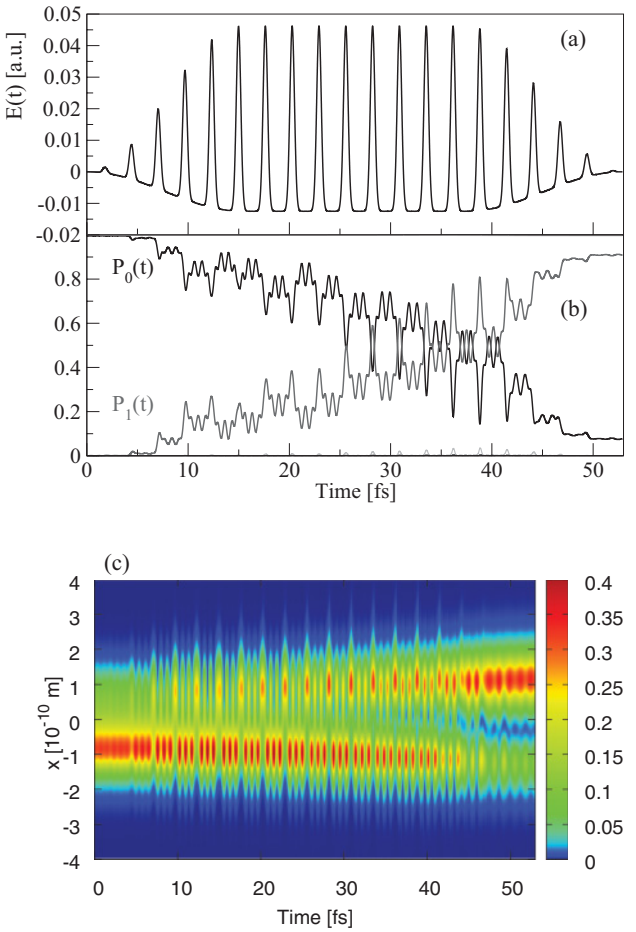

FIG. 13. (Color online) (a) Evolution of the polar molecule driven by the optimized HCP train: (b) population transfer dynamics and (c) electronic density $\varrho(x,t)$.

Fig. 4, almost identical localization dynamics can be obtained (see Fig. 14). The modulation on top of the electronic dynamics due to the vibrational motion is, of course, different as both systems have a different reduced mass.

Following our earlier investigations on the control of electron localization in the course of dissociation of H_2^+ [25], we have also investigated the possibility to control electron localization in dissociative systems with different masses. We have compared the electronic dynamics in H_2^+ with the isotopes HD^+ and DH^+. Here, too, despite the fact that the heterodiatomic systems have a different dipole interaction term [see Eq. (4)], the same HCP field, which was able to induce electron localization in H_2^+, also steers the electronic dynamics in the isotopic heteronuclear systems with almost the same efficiency (Fig. 14).

C. Localization in a model system with four nuclei

As a first step toward controlling electronic dynamics in chainlike molecules, we examine localization dynamics in a potential mimicking a four-atomic linear molecule. For demonstration purposes, we restrict ourselves to a simplified test system with frozen nuclear coordinates. The one-electron

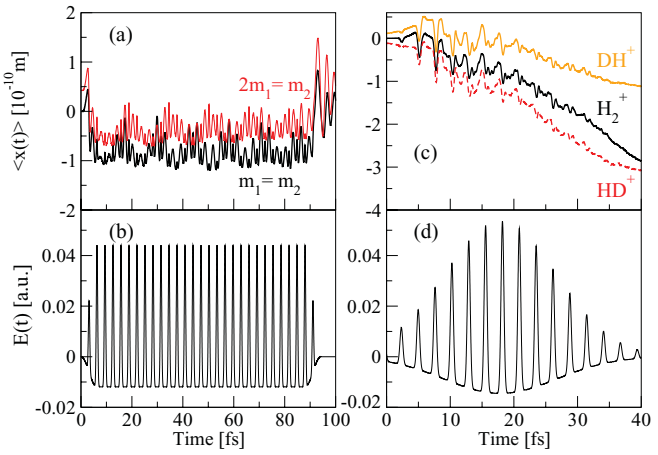

FIG. 14. (Color online) Comparison of the electron expectation values $\langle x(t)\rangle$ of the heteronuclear molecules [upper panels: (a), (c)] driven by the HCP trains shown below [lower panels: (b), (d)]. Left column: (a) model system (I) with two nuclei of the same isotope (black line) and with different isotopes (red line) driven by (b) the pulse train (same as in Fig. 4). Right column: (c) dissociative model systems of H_2^+, HD^+, and DH^+ driven by (d) the pulse train.

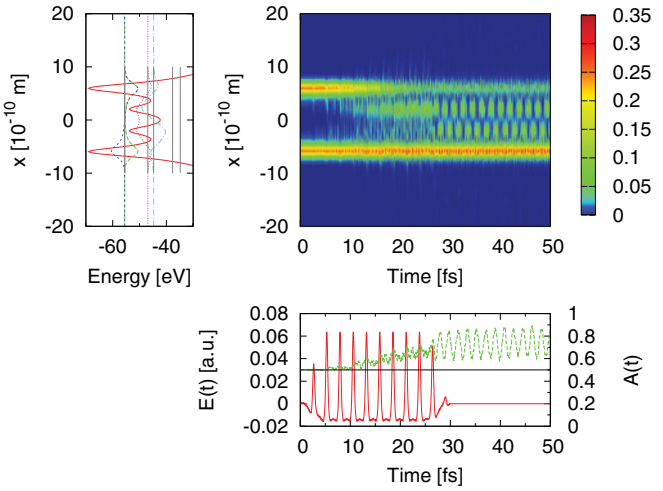

FIG. 15. (Color online) Upper left panel: electronic potential and lowest eigenstates of a model system with four nuclei. Middle panel: electronic density $\varrho(x,t)$, driven by an optimized pulse train (solid line) in the lower panel. The lower panel also displays the asymmetry $A(t)$ (thin dashed line). The pulse train leaves the system in a coherent superposition of electronic states.

Hamiltonian is given by

$$H = \hat{T}_x - \frac{1}{\sqrt{(x \pm R/2)^2 + \alpha}} - \frac{2}{\sqrt{(x \pm 3R/2)^2 + \alpha}}. \quad (17)$$

The internuclear distance is fixed to $R = 4$ a.u., and the screening parameter α is set to 1. The electronic potential, as well as the lowest electronic eigenstates and eigen energies are shown in Fig. 15 (left panel). In Fig. 15, the HCP train pushes the electron density being initially localized mainly in the outer, deeper potential wells over the internuclear barrier to the left potential well. During interaction, the lowest electronic states are excited. From Fig. 15 it can be gathered that after the end of the pulse train, the system is in a superposition state of the lowest electronics eigenstates. The electron density is mainly localized in the left outer (deeper) potential well, with clearly visible oscillations in between the two middle potential wells.

While this reduced system does not fully describe the charge transfer dynamics in chainlike molecules as the vibrational motion is not included, the example suggests that controlled charge migration in larger systems is possible and proceeds under similar conditions as we have analyzed for the diatomic molecules.

IV. SUMMARY AND CONCLUSION

Motivated by the recent experimental advances in the production of strong multicycle laser fields breaking inversion symmetry, we investigated the prospects of using such fields to control bound state dynamics in small molecules. Two types of unidirectional fields have been considered. One type is trains of unidirectional half-cycle pulses on the few femtosecond scale. Such trains consist of narrow "spikes" in one direction and a weak offset field in the opposite direction. For comparison, we considered the dynamics induced by the offset field only. Such a pulse can be considered as a half cycle of an (almost) one color field with a very low frequency resembling a terahertz pulse.

We have presented numerical simulations examining the control of electron localization in bound prototype molecular model systems. Extending our recent work [25], the systems we have analyzed here are not dissociative, excluding from the very beginning the freezing out of electronic motion during dissociation.

We explore the mechanism leading to localization in three different model potentials. In model system (I), the almost static offset component of the field shapes field-dressed Born-Oppenheimer potential curves. Between the kicks, the system adiabatically follows the dressed states, while the HCPs induce almost impulsive couplings between the states. We have shown that the first kicks during the ramp-on of the field induce population inversion into the lowest lying field-dressed vibrational state in the upper electronic state in which the system stays for long times. The almost identical shape of the upper and lower potential curves enables long-term synchronous nuclear dynamics in both states which, in turn, leads to a high degree of asymmetry lasting over several vibrational periods. Model system (II) features a wide excitation gap and different equilibrium internuclear distances in the two electronic states. The best field found induces localization as soon as the nuclear wave packets in the lower and upper electronic state approach the outer turning point where the gap between the states is reduced. Applying the offset component with a smooth turning on and off (a terahertz pulse) only yields in all cases a high degree of localization. Model system (III), mimicking heterodiatomic molecules, enables permanent localization of the electron as population inversion implies switching of the preferred nuclear site. We found the population inversion to proceed via stepwise population transfer.

Although for the homonuclear diatomic molecules localization exists only in the presence of the field, this is a necessary

precursor for the implementation of electron-charge transfer along chainlike molecules. Transient polarization can induce a molecular electronic current from one end of the chain to the other. Furthermore, detachment of selected functional groups via electron localization and bond breaking can be envisioned. Transient electron localization can be probed via the asymmetry in the photoelectron distribution induced by a weak, attosecond XUV pulse [40]. Details of such a probe will be shown in a future publication.

ACKNOWLEDGMENTS

For the optimization, the GAlib genetic algorithm package (written by Matthew Wall at the Massachusetts Institute of Technology) was used. This work was supported by the Austrian Science Foundation FWF Project No. 21141-N16 (E.P., G.W.). G.W. also acknowledges funding by the International Max-Planck Research School APS. S.G. acknowledges FWF support within the Lise-Meitner Program, Project No. M1077-N16.

[1] W. S. Warren, H. Rabitz, and M. Dahleh, Science **259**, 1581 (1993).

[2] H. Rabitz, R. de Vivie-Riedle, M. Motzkus, and K.-L. Kompa, Science **288**, 824 (2000).

[3] M. Shapiro and P. Brumer, *Principles of Quantum Control of Molecular Processes* (Wiley, New York, 2003).

[4] S. A. Rice and M. Zhao, *Optical Control of Molecular Dynamics* (Wiley, New York, 2000).

[5] T. Brixner, N. H. Damrauer, and G. Gerber, Adv. At. Molec. Opt. Phys. **46**, 1 (2001).

[6] M. Dantus and V. V. Lozovoy, Chem. Rev. **104**, 1813 (2004).

[7] M. Wollenhaupt, A. Assion, and T. Baumert, *Springer Handbook of Optics* (Springer, Heidelberg, 2004).

[8] N. Dudovic, O. Smirnova, J. Levesque, Y. Mairesse, M. Yu. Ivanov, D. M. Villeneuve, and P. B. Corkum, Nat. Phys. **2**, 781 (2006).

[9] X. Xie, S. Roither, D. Kartashov, E. Persson, D. G. Arbó, L. Zhang, S. Gräfe, M. S. Schöffler, J. Burgdörfer, A. Baltuska, and M. Kitzler (unpublished).

[10] Y. Mairesse, N. Dudovic, J. Levesque, M. Yu. Ivanov, P. B. Corkum, and D. M. Villeneuve, New J. Phys. **10**, 025015 (2006).

[11] I. J. Sola *et al.*, Nat. Phys. **2**, 319 (2006).

[12] M. Wollenhaupt, A. Präkelt, C. Sarpe-Tudoran, D. Liese, and T. Baumert, Appl. Phys. B **82**, 183 (2006).

[13] J. R. Kuklinski, U. Gaubatz, F. T. Hioe, and K. Bergmann, Phys. Rev. A **40**, 6741 (1989).

[14] C. Trallero-Herrero, D. Cardoza, T. C. Weinacht, and J. L. Cohen, Phys. Rev. A **71**, 013423 (2005).

[15] B. J. Sussman, M. Y. Ivanov, and A. Stolow, Phys. Rev. A **71**, 051401(R) (2005).

[16] M. F. Kling *et al.*, Science **312**, 246 (2006).

[17] C. Uiberacker and W. Jakubetz, J. Chem. Phys. **120**, 11532 (2004).

[18] N. Elghobashi and L. González, Phys. Chem. Chem. Phys. **6**, 4071 (2004).

[19] D. Geppert, P. von den Hoff, and R. de Vivie-Riedle, J. Phys. B: At. Mol. Phys. **41**, 074006 (2008).

[20] F. He, C. Ruiz, and A. Becker, Phys. Rev. Lett. **99**, 083002 (2007).

[21] F. He, C. Ruiz, and A. Becker, J. Phys. B: At. Mol. Phys. **41**, 081003 (2008).

[22] X. M. Tong and C. D. Lin, Phys. Rev. Lett. **98**, 123002 (2007).

[23] S. Gräfe and M. Y. Ivanov, Phys. Rev. Lett. **99**, 163603 (2007).

[24] S. Gräfe and M. Y. Ivanov, J. Mod. Opt. **55**, 2557 (2008).

[25] E. Persson, J. Burgdörfer, and S. Gräfe, New J. Phys. **11**, 105035 (2009).

[26] C. R. Calvert, W. A. Bryan, W. R. Newell, and I. D. Williams, Phys. Rep. **491**, 1 (2010).

[27] S. Gräfe and V. Engel, Chem. Phys. **329**, 118 (2006).

[28] G. G. Paulus, F. Grasbon, H. Walter, P. Villoresi, M. Nisoli, S. Stagira, E. Priori, and S. De Silvestri, Nature (London) **414**, 182 (2001).

[29] D. G. Arbó, E. Persson, and J. Burgdörfer, Phys. Rev. A **74**, 063407 (2006).

[30] R. Gopal *et al.*, Phys. Rev. Lett. **103**, 053001 (2009).

[31] M. V. Korolkov, J. Manz, and G. K. Paramonov, Chem. Phys. **217**, 341 (1997).

[32] N. Elghobashi, P. Krause, J. Manz, and M. Oppel, Phys. Chem. Chem. Phys. **5**, 4806 (2003).

[33] C. Uiberacker and W. Jakubetz, J. Chem. Phys. **120**, 11540 (2004).

[34] C. M. Dion, A. Keller, and O. Atabek, Euro. Phys. J. D **14**, 249 (2001).

[35] A. Matos-Abiague and J. Berakdar, Chem. Phys. Lett. **382**, 475 (2003).

[36] C. O. Reinhold, J. Burgdörfer, M. T. Frey, and F. B. Dunning, Phys. Rev. Lett. **79**, 5226 (1997).

[37] M. T. Frey, F. B. Dunning, C. O. Reinhold, S. Yoshida, and J. Burgdörfer, Phys. Rev. A **59**, 1434 (1999).

[38] B. E. Tannian, C. L. Stokely, F. B. Dunning, C. O. Reinhold, S. Yoshida, and J. Burgdörfer, Phys. Rev. A **62**, 043402 (2000).

[39] E. Persson, S. Yoshida, X. M. Tong, C. O. Reinhold, and J. Burgdörfer, Phys. Rev. A **68**, 063406 (2003).

[40] S. Gräfe, V. Engel, and M. Y. Ivanov, Phys. Rev. Lett. **101**, 103001 (2008).

[41] M. D. Feit, J. A. Fleck, and A. Steiger, J. Comput. Phys. **47**, 412 (1982).

[42] E. Persson, S. Puschkarski, X.-M. Tong, and J. Burgdörfer, in *Ultrafast Optics* IV, edited by F. Krausz *et al.*, Springer Series in Optical Sciences Vol. 95 (Springer, New York, 2004), p. 253.

[43] E. Persson, K. Schiessl, A. Scrinzi, and J. Burgdörfer, Phys. Rev. A **74**, 013818 (2006).

[44] M. Y. Shverdin, D. R. Walker, D. D. Yavuz, G. Y. Yin, and S. E. Harris, Phys. Rev. Lett. **94**, 033904 (2005).

[45] W.-J. Chen *et al.*, Phys. Rev. Lett. **100**, 163906 (2008).

[46] G. N. Gibson, Phys. Rev. Lett. **89**, 263001 (2002).

[47] S. Gräfe, M. Erdmann, and V. Engel, Phys. Rev. A **72**, 013404 (2005).